[논 문] 한국재료학회지
Korean J. Mater. Res.
Vol. 33, No. 9 (2023)

https://doi.org/10.3740/MRSK.2023.33.9.367

Preparation and Structure Properties of $LaBa_2Cu_2O_9$, $LaBa_2CaCu_3O_{12}$ and $LaBa_2Ca_2Cu_5O_{15}$ Perovskites

Kareem Ali Jasim, Hind Abdulmajeed Mahdi†, Rafah Ismael Noori, and Marwa Ayad Abdulmajeed

Department of Physics, College of Education for Pure Science (Ibn Al-Haitham), University of Baghdad, Baghdad 10001, Iraq

(Received August 14, 2023 : Revised September 17, 2023 : Accepted September 18, 2023)

Abstract In this study we examine variations in the structure of perovskite compounds of $LaBa_2Cu_2O_9$, $LaBa_2CaCu_3O_{12}$ and $LaBa_2Ca_2Cu_5O_{15}$ synthesized using the solid state reaction method. The samples' compositions were assessed using X-ray fluorescence (XRF) analysis. The La: Ba: Ca: Cu ratios for samples $LaBa_2Cu_2O_9$, $LaBa_2CaCu_3O_{12}$ and $LaBa_2Ca_2Cu_5O_{15}$ were found by XRF analysis to be around 1:2:0:2, 1:2:1:3, and 1:2:2:5, respectively. The samples' well-known structures were then analyzed using X-ray diffraction. The three samples largely consist of phases 1202, 1213, and 1225, with a trace quantity of an unknown secondary phase, based on the intensities and locations of the diffraction peaks. According to the measured parameters a, b, and c, every sample has a tetragonal symmetry structure. Each sample's mass density was observed to alter as the lead oxide content rose. Scanning electron microscope (SEM) images of the three phases revealed that different Ca-O and Cu-O layers can cause different grain sizes, characterized by elongated thin grains, without a preferred orientation.

Key words X-ray diffraction, tetragonal symmetry structure, X-ray fluorescence, scanning electron microscope, mass density and grain sizes.

1. Introduction

Perovskite materials have a wide range of physical and chemical properties. Due to their extremely flexible structural possibilities, these materials exhibit a wide range of electrical and magnetic activity. Their wide-ranging uses span a variety of disciplinary domains, including optoelectronic and photochromic applications, industrial electrical uses, energy-related uses, and diverse sectors of sensors, biosensors, and catalysts. The general formula for perovskites is ABX_3,[1] where X can either be oxygen or a halogen, and A and B are cations. They fall under the perovskite oxide or perovskite halide family based on this. Gustav Rose found the first perovskite, $CaTiO_3$, in 1839, and Count Le Alexerch von Perovskite was the inspiration for the name "perovskite".[2-4] According to the reports, perovskite materials exhibit insulator, semiconductor, metal, and superconductor activity. Surface acoustic wave signal processing, switching, and filtering devices are among the areas in which they have applications.[5] Heterogeneous catalysis of nitrogen oxide reductions is one of the industrial applications of perovskite materials as a catalyst.[6-9] These substances are known as cleaning catalysts because they are utilized in car exhaust gas catalysts to selectively remove impurities from gaseous mixtures. Perovskite materials can also catalyze oxygen evolution reactions and oxygen reduction reactions, which are employed in fuel cells, rechargeable batteries, water electrolysis, the production of organic compounds, and rechargeable batteries.[10] Additionally, these substances are employed in hydrogen evolution processes. The topic of sensors and biological sensors has seen a wide range of research.[11,12] Perovskite has been used in a number of studies as a gas sensor and neurotransmitter sensor. The perovskite materials have also aided research into fuel cells and solar cells.[13] The optoelectronic and photovoltaic uses

†Corresponding author
E-Mail : hind.a.m@ihcoedu.uobaghdad.edu.iq (H. A. Mahdi, Univ. Baghdad)

of metal halide perovskites are well recognized.[14,15] Multi-perovskite compounds, composed of layers of perovskite swapping atoms at the sites between the layers, make up the crystal structure of superconducting substances. The oxide of lanthanum, barium, and copper is one of these substances.[16-20]

The preparation of a Lanthanum-barium-copper oxide compound, abbreviated as LBCO and examination of the structural characteristics of its three phases ($LaBa_2Cu_2O_9$, $LaBa_2CaCu_3O_{12}$ and $LaBa_2Ca_2Cu_5O_{15}$) will be the main topics of this article.

2. Experimental

The polycrystalline $LaBa_2Cu_2O_9$, $LaBa_2CaCu_3O_{12}$ and $LaBa_2Ca_2Cu_5O_{15}$ samples were prepared using a solid-state reaction technique from the nominal starting compositions of high purity oxides (99.99 %) with appropriate proportions of LaO, CaO, BaO and CuO. The oxides were mixed using an electric mixer for an hour in order to obtain a homogeneous mixture. For the three vehicles. And heated at 820 °C. For more than 8 h. The heated precursor was then thoroughly combined and formed into pellets with the dimensions of 15 mm in diameter and 3 mm in thickness. The pellets underwent a 48 h, 950 °C furnace heating and 48 h, room-temperature cooling process. The pellets were heating in the furnace at 950 °C for 48 h and cooled by the same rate at room-temperature. Samples were tested using X-ray diffraction technique (Philips) with the following properties: source current $Cu_{k\alpha}$ (20 mA), voltage (40 KV), and λ = 1.5405 Å. Lattice parameters a, b and c were calculated by using a computer program based (Cohen's least squares method). Scanning electron microscope (Philips XL 30) to examine the surface topography of the samples.

3. Results and Discussion

X-ray fluorescence (XRF) analysis was used to evaluate the $LaBa_2Cu_2O_9$, $LaBa_2CaCu_3O_{12}$ and $LaBa_2Ca_2Cu_5O_{15}$, composition of the samples. The results are displayed in Fig. 1. The samples' XRF examination reveals that the ratios of La: Ba: Ca: Cu are approximately 1:2:0:2, 1:2:1:3, and 1:2:2:5. for the samples $LaBa_2Cu_2O_9$, $LaBa_2CaCu_3O_{12}$ and $LaBa_2Ca_2Cu_5O_{15}$, respectively.

The well-known structures of $LaBa_2Cu_2O_9$, $LaBa_2CaCu_3O_{12}$ and $LaBa_2Ca_2Cu_5O_{15}$ phases were tested by X-ray diffraction. The X-ray diffraction patterns powder of laboratory-prepared 1202, 1213, and 1225 phases are displayed in Fig. 2. The three samples were found to primarily consist of the primary phases 1202, 1213, and 1225, with a minor amount of an unidentified secondary phase also present, according to the intensities and positions of the diffraction peaks.

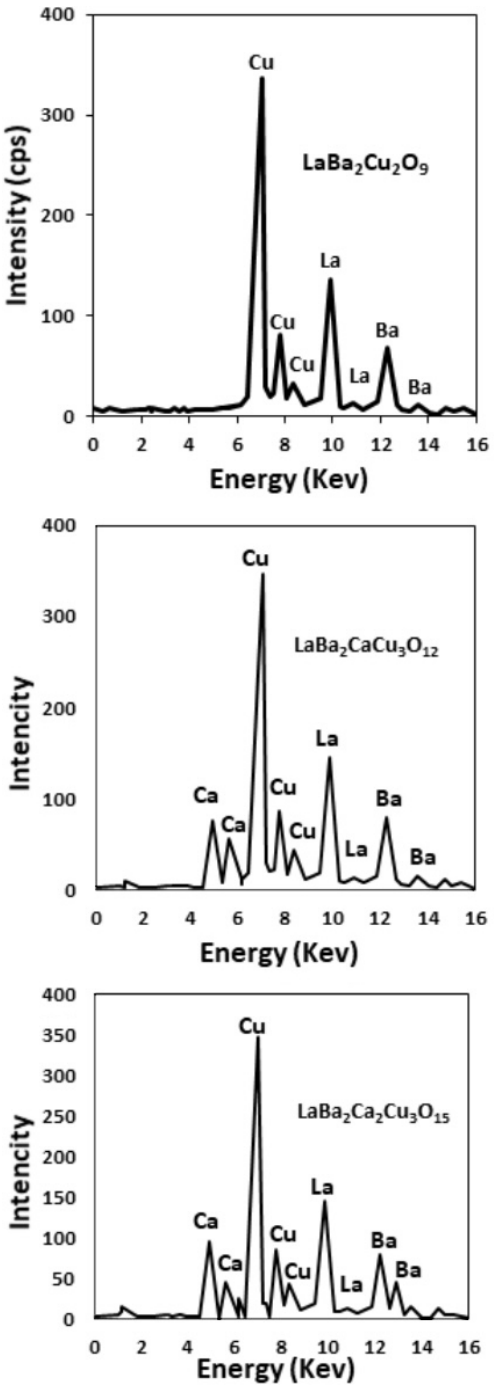

Fig. 1. shown the XRF patterns of $LaBa_2Cu_2O_9$, $LaBa_2CaCu_3O_{12}$ and $LaBa_2Ca_2Cu_5O_{15}$ samples.

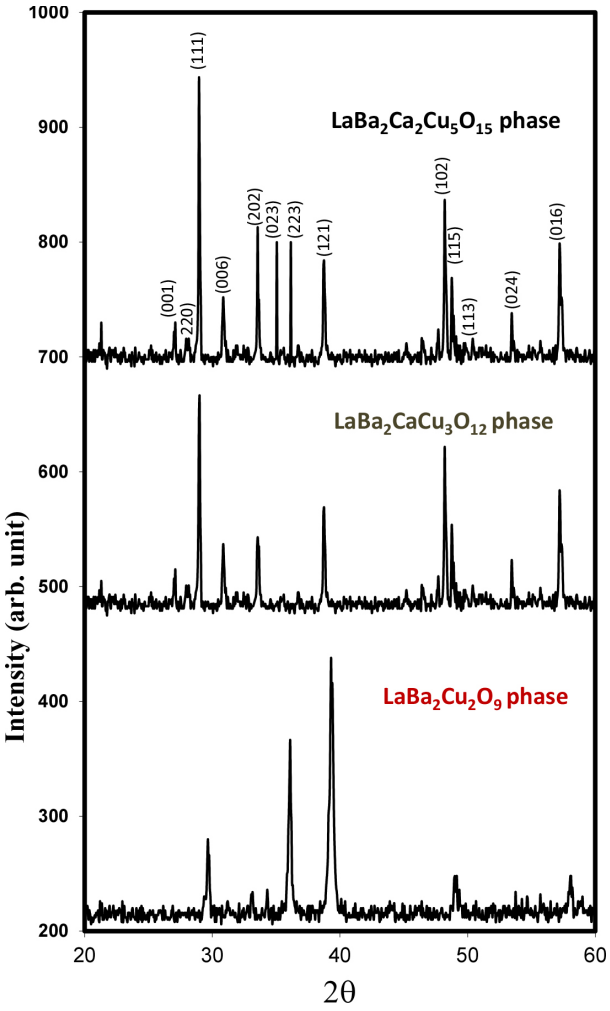

Fig. 2. $LaBa_2Cu_2O_9$, $LaBa_2CaCu_3O_{12}$ and $LaBa_2Ca_2Cu_5O_{15}$ samples XRD patterns.

A Cohen's least squares-based algorithm was used to determine the lattice parameters for phases 1202, 1213, and 1225 using the (hkl) reflections and d values of observed X-ray diffraction patterns.[21,22] All of our samples exhibit a tetragonal symmetry structure according to the measured parameters a, b, c, and ratio c/a. Along with the crystal lattice parameters a, b, and c and the ratio c/a, the mass density of each sample was also computed and presented in Table 1.

Fig. 3 illustrates the relationship between mass density and calcium concentration. It was shown from this figure that the increase increasing calcium content produced high mass density M, due to the growth of layers of calcium and copper oxides in the crystal structure, which caused an increase in the mass density with an increase in calcium concentration.[23-26]

The crystal structure of the three samples $LaBa_2Cu_2O_9$, $LaBa_2CaCu_3O_{12}$ and $LaBa_2Ca_2Cu_5O_{15}$ are shown in Fig. 4, which was drawn based on the intensity values and individual X-ray diffraction angles taken in the XRD pattern using Full-Prof software. This figure shows the effect of increasing calcium and copper layers along the c-axis.[27,28]

Fig. 5 displays SEM images of the $LaBa_2Cu_2O_9$, $LaBa_2CaCu_3O_{12}$ and $LaBa_2Ca_2Cu_5O_{15}$ phases. It is discovered that different Ca-O and Cu-O layers cause different grain sizes which were calculated using the scale shown at the bottom of Fig. 5. Within the limits of Scanning electron microscope

Table 1. Values of crystal lattice parameters a, b, and c, ratio c/a, the mass density for $LaBa_2Cu_2O_9$, $LaBa_2CaCu_3O_{12}$ and $LaBa_2Ca_2Cu_5O_{15}$ samples.

Phases	Samples	a (Å)	b (Å)	c (Å)	c/a	Mass density (g/cm^3)
1202	$LaBa_2Cu_2O_9$	3.72	3.72	10.892	2.490	6.15
1213	$LaBa_2CaCu_3O_{12}$	3.86	3.86	15.586	3.306	6.47
1235	$LaBa_2Ca_2Cu_5O_{15}$	3.65	3.65	21.679	4.146	6.62

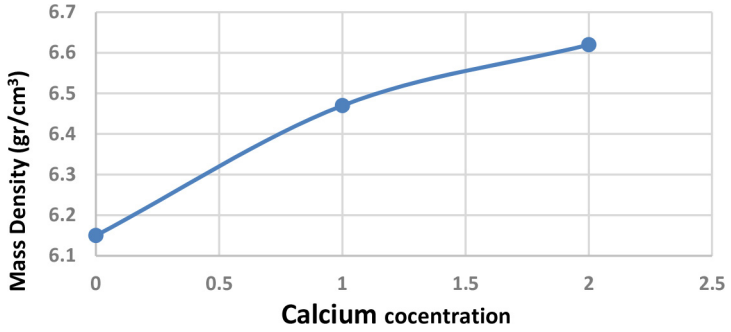

Fig. 3. Calcium concentration as function density of mass for $LaBa_2Cu_2O_9$, $LaBa_2CaCu_3O_{12}$ and $LaBa_2Ca_2Cu_5O_{15}$ samples.

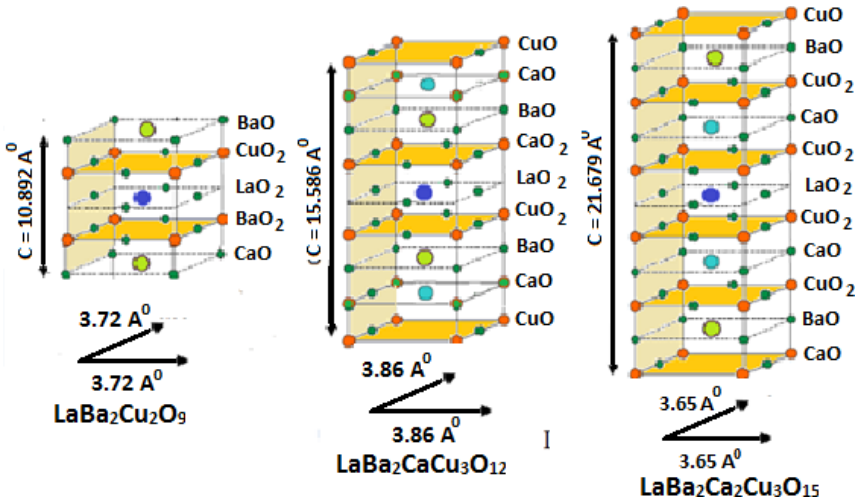

Fig. 4. Crystal structure of the $LaBa_2Cu_2O_9$, $LaBa_2CaCu_3O_{12}$ and $LaBa_2Ca_2Cu_5O_{15}$ samples.

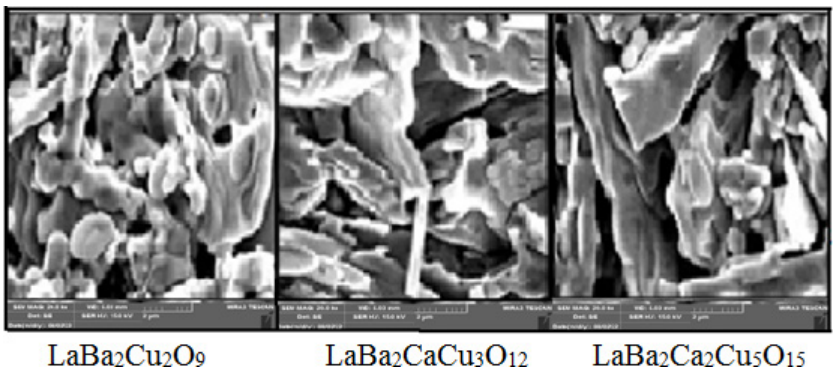

Fig. 5. shows SEM images of the $LaBa_2Cu_2O_9$, $LaBa_2CaCu_3O_{12}$ and $LaBa_2Ca_2Cu_5O_{15}$ phases taken SEM Microscope.

(SEM) magnification, this figure depicts formation of the three phases, each of which is the characterized by thin, elongated grains without the preferred orientation.[29,30] According to Table 1, the 1225 phase specimen contained larger grains than those of the 1202 and 1213 phases because of an increase in contact areas, which results in a higher density.[31]

4. Conclusions

Three of $LaBa_2Cu_2O_9$, $LaBa_2CaCu_3O_{12}$ and $LaBa_2Ca_2Cu_5O_{15}$ phases were prepared by the solid-state reaction method. Changes are made to the values of the mass density and the lattice parameters (a, b, c, and c/a) by increasing calcium concentration. All samples according to XRD examination, have a tetragonal structure. The ratio c/a of the lattice parameters and c-axis lattice constant both increased as the Cu-O layers number increased. secondary electron SEM images of the phases discovered that increasing in the Ca-O and Cu-O layers cause different grain sizes, within the limits of SEM magnification.

References

1. T. Wolfram and S. Ellialtioglu, Electronic and optical properties of D-BanD perovskites, p.1, Cambridge University Press, Cambridge (2006).
2. F. S. Galasso, Structure of perovskite-type compounds, 1st ed., p.3-49, Pergamon Press, New York (1969).
3. K. A. Jassim, W. H. Jassim and S. H. Mahdi, Energy Procedia, **119**, 650 (2017).
4. T. Lindemer, B. Chakoumakos, E. Specht, R. Williams and Y. Chen, Phys. C, **231**, 80 (1994).
5. K. A. Jasim, S. A. Makki and A. A. Almohsin, Physics Procedia, **55**, 336 (2014).
6. T. Ishihara, Structure and properties of perovskite oxides, p. 1-16, Springer, Boston (2009).
7. A. Galal, N. F. Atta and S. M. Ali, Electrochim. Acta, **56**, 5722 (2011).

8. H. A. Mahdi, K. A. Jasim and A. H. Shaban, Energy Procedia, **157**, 158 (2019).
9. S. Malkhandi, A. K. Manohar, B. Yang, G. K. S. Prakash and S. R. Narayanan, ECS Meeting Abstracts, **MA2011-02**, 292 (2011).
10. A. Kahoul, A. Hammouche, F. Nâamoune, P. Chartier, G. Poillerat and J. Koenig, Mater. Res. Bull., **35**, 1955 (2000).
11. S. M. Haile, Acta Mater., **51**, 5981 (2003).
12. M. Ghasdi and H. Alamdari, Sens. Actuators, B, **148**, 478 (2010).
13. G. Wang, J. Sun, W. Zhang, S. Jiao and B. Fang, Microchim. Acta, **164**, 357 (2008).
14. R. Wang, J. Wu, S. Wei, J. Zhu, M. Guo, Q. Zheng, M. Wei and S. Cheng, J. Power Sources, **544**, 231870 (2022).
15. R. Seshadri, V. Manivannan, K. Rajeev, J. Gopalakrishnan and C. Rao, J. Solid State Chem., **89**, 389 (1990).
16. K. A. Jasim and R. S. Al-Khafaji, J. Phys.: Conf. Ser., **1003**, 012096 (2018).
17. H. M. Haider and K. A. Jasim, Ibn Al-Haitham J. Pure Appl. Sci., **33**, 17 (2020).
18. K. A. Jasim and L. A. Mohammed, J. Phys.: Conf. Ser., **1003**, 012071 (2018).
19. L. A. Mohammed and K. A. Jasim, Energy Procedia, **157**, 135 (2019).
20. B. A. Omar, S. J. Fathi and K. A. Jassim, AIP Conf. Proc., **1968**, 030047 (2018).
21. S. Funaki, Y. Ichino, Y. Yoshida, K. Inoue, Y. Takai, K. Matsumoto, M. Mukaida, A. Ichinose and S. Horii, Phys. C, **468**, 1575 (2008).
22. K. A. Jasim, Turk. J. Phys., **36**, 245 (2012).
23. Y. Ichino, Y. Yoshida, K. Inoue, S. Funaki, Y. Takai, K. Matsumoto, M. Mukaida, A. Ichinose and S. Horii, Phys. C, **468**, 1623 (2008).
24. K. A. Jasim, J. Supercond. Novel Magn., **26**, 549 (2012).
25. A. Ichinose and A. Shirabe, Phys. C, **277**, 243 (1997).
26. K. A. Jasim and L. A. Mohammed, J. Phys.: Conf. Ser., **1003**, 012071 (2018).
27. M. Radhi Jobayr, S. H. Mahdi, E. M. Salman and K. A. Jasim, J. Ovonic Res., **18**, 357 (2018).
28. B. Aslibeiki, P. Kameli and H. Salamati, Iran. J. Phys. Res., **16**, 251 (2017).
29. K. A. Jasim, Turk. J. Phys., **37**, 237 (2013).
30. H. M. Haider, K. M. Wadi, H. A. Mahdi, K. A. Jasim and A. H. Shaban, AIP Conf. Proc., **2123**, 020033 (2019).
31. S. Funaki, Y. Yoshida, Y. Ichino, M. Miura, Y. Takai, K. Matsumoto, A. Ichinose, M. Mukaida and S. Horii, Phys. C, **463-465**, 644 (2007).

Author Information

Kareem Ali Jasim
Professor, Department of Physics, College of Education for Pure Science (Ibn Al-Haitham), University of Baghdad

Hind Abdulmajeed Mahdi
Assistant Professor, Department of Physics, College of Education for Pure Science (Ibn Al-Haitham), University of Baghdad

Rafah Ismael Noori
Lecturer, Department of Physics, College of Education for Pure Science (Ibn Al-Haitham), University of Baghdad

Marwa Ayad Abdulmajeed
Lecturer, Department of Physics, College of Education for Pure Science (Ibn Al-Haitham), University of Baghdad